PAPER • OPEN ACCESS

Dynamical suppression of Coulomb interaction and sub-fs jitter correction in electron pulse compression

New Journal of Physics
The open access journal at the forefront of physics

Deutsche Physikalische Gesellschaft DPG
IOP Institute of Physics

Published in partnership with: Deutsche Physikalische Gesellschaft and the Institute of Physics

OPEN ACCESS

RECEIVED
20 May 2020

REVISED
14 July 2020

ACCEPTED FOR PUBLICATION
29 July 2020

PUBLISHED
1 September 2020

PAPER

Dynamical suppression of Coulomb interaction and sub-fs jitter correction in electron pulse compression

Yingpeng Qi[1,2,3,7], Yan Yang[1], Haitao Sun[1,4], Xuan Wang[5], Jianming Cao[3,6], Ralph Ernstorfer[2] and Zhenrong Sun[1,4,7]

[1] State Key Laboratory of Precision Spectroscopy, East China Normal University, Shanghai 200062, People's Republic of China
[2] Fritz-Haber-Institut der Max-Planck-Gesellschaft, Faradayweg 4-6, Berlin 14195, Germany
[3] Center for Ultrafast Science and Technology, School of Physics and Astronomy, Shanghai Jiao Tong University, Shanghai 200240, People's Republic of China
[4] Collaborative Innovation Center of Extreme Optics, Shanxi University, Taiyuan, Shanxi 030006, People's Republic of China
[5] Beijing National Laboratory for Condensed Matter Physics, Institute of Physics, Chinese Academy of Sciences, Beijing 100190, People's Republic of China
[6] Physics Department and National High Magnetic Field Laboratory, Florida State University, Florida 32310, United States of America
[7] Authors to whom any correspondence should be addressed.

E-mail: qiyp@sjtu.edu.cn and zrsun@phy.ecnu.edu.cn

Keywords: ultrafast electron diffraction, Coulomb interaction, jitter correction, electron pulse compression

Abstract

Achieving a few-femtosecond (fs) temporal resolution in electron diffraction and electron microscopy is essential for directly tracking the electronic processes and the fastest atomic motions in molecule and condensed matter systems. The intrinsic Coulomb interaction among electrons broadens the pulse duration and restricts the temporal resolution. To tackle this issue, the electron pulse compression by the time-varying electric fields at optical, THz and RF wavelengths has been demonstrated recently. However, the Coulomb interaction still exists in the compression process and the impact of the Coulomb interaction to the compression remains largely unaccounted for. In this work, we quantify the impact of the Coulomb interaction and present three intrinsic characters of Coulomb interaction in the compression process: the Coulomb interaction is dynamically suppressed as the compression field strength rises; the electron pulse with arbitrary kinetic energy (eV to MeV) suffers the same amount of Coulomb interaction, i.e. the Coulomb interaction is independent on the kinetic energy in compression; the dynamical suppression of Coulomb interaction within a single pulse gives rise to a dispersion of the temporal focus and impedes the further compression to attosecond. Potential applications based on the revealed characters of the Coulomb interaction in the compression process are discussed. Based on the dynamical evolution of the Coulomb interaction, three stages are identified to describe the compression process, which is beyond the ballistic compression model. Additionally, a robust and noninvasive jitter correction approach matching well with the compression regime is presented and the proof-of-principle experiment demonstrates a sub-fs accuracy.

1. Introduction

Ultrafast electron and x-ray diffractions [1, 2] provide a four-dimensional visualization of the atomic-level structural dynamics in chemical, biological and material science by taking snapshots of transient structures with ultrashort electron and x-ray pulses. Using these direct and ultrafast structural probes, complex phase diagrams and structural transitions resulted from the mutual interactions among the lattice [3–5], electron [6, 7], spin and orbital [8] can be distinguished and examined in real time. Recently the single-spike hard x-ray pulse with a nonlinear electron pulse compression advances the temporal resolution to the 200 attosecond timescale [9]. Complementary to the ultrafast x-ray diffraction, ultrafast electron diffraction (UED) with a beam energy ranging from hundreds of eV to a few MeV [10] has also been developed and widely used for resolving atomic-scale structural dynamics, largely due to its relatively lower expense and

flexible tabletop implementation. However, achieving a temporal resolution better than a few femtoseconds (fs) for directly observing the fastest atom rearrangement even the electron dynamics in the molecules and the condensed matter systems, is still a big challenge.

The inherent Coulomb repulsive force in an electron pulse expands the pulse duration as it moves from the source to the sample. To mitigate the Coulomb expansion, both compact keV UED [10–14] and higher MeV [15] beam energy UED schemes are explored in the past decades, the former minimizes the traveling time from the source to the sample and the later utilizes the relativistic effect to shorten the pulse duration. Alternatively, a compression regime, verified firstly in the radio frequency (RF) gun accelerator system [16], was proposed which is termed as the ballistic compression model. The ballistic compression model gives a general concept for the compression process that the tail electrons in a pulse gain more energy than that of the head electrons from the compression field, and subsequently the tail electrons catch up the front electrons at the temporal focus position, resulting a compressed and shorter pulse. The subsequent enormous success in the community of electron pulse compression has been achieved, especially the recent compression of electron pulses to the 10 fs level by the optical, THz and RF fields [17–31]. Notably, concomitant with the electron pulse compression, the Coulomb interaction still exists in the compression process, however, it was neglected in the ballistic compression model [16] and the analytical model [26]. A recent experimental study reveals that the Coulomb interaction in the compression process can induce the elongation of temporal focus and give rise to a jitter amplification effect [31], which cannot be accounted for by the ballistic compression model [16] and the analytical model [26]. A modified model based on the ballistic compression model, which involves the Coulomb interaction qualitatively in the compression process, has been proposed recently [28, 29]. This modified model, which is named as the energy transformation model in this work, treats the compression as a reverse process of the Coulomb expansion in the free propagation. It assumes that the energy chirp gained from the compression field transforms to the Coulomb potential energy at the temporal focus, mimicking the initial state right after the photoemission. However, a recent experimental study [30] reveals that there is no such significant energy transformation at the temporal focus. Moreover, the energy transformation model indicates a compression back to the duration of the photoemission laser [28], thus it fails in depicting a drastic compression scenario where the electron pulse is compressed to far below the pulse duration of the photoemission laser. Therefore, it is necessary to revisit the compression regime by taking into account the Coulomb interaction for an elaborate control of electron pulses, in particular for compressing electron pulses to the attosecond timescale.

Besides the pulse duration, the timing jitter between the pump laser and the compressed electron pulse also contributes significantly to the overall temporal resolution. The phase and the amplitude fluctuations of the compression field change the kinetic energy of the electron pulse and the energy shift will in turn change the arrival time of the electron pulse relative to the pump laser at the sample position. An accurate long term synchronization with sub-10 fs root mean square (RMS) jitter between the laser oscillator and the electron pulse has been achieved recently [32, 33]. The additive timing jitter from the regenerative amplifier [34], the fluctuations of the RF power, the environment temperature and the humidity will degenerate the precision of this synchronization in high-charge electron pulse compression [30, 35–37]. By compensating the phase shift in the RF cavity, a long term synchronization (<50 fs RMS) has been reported in the compression of 10^6 electrons [38]. Indeed, even in the compression with THz field, where the synchronization between the electron pulse and the THz pulse is inherently guaranteed, a 4 fs RMS jitter arises [23]. A promising approach, which can effectively correct the aforementioned overall jitter, is the post processing by time stamping. Such jitter correction approaches have been explored in both x-ray FEL [39, 40] and UED [32, 41, 42] communities. However, these approaches, either introducing distortion in the diffraction pattern [41] or cannot be readily extended to high-charge electron pulse compression setup [32]. A more general, robust and non-invasive jitter correction approach with high enough precision is in demand.

In this work, we reveal three intrinsic characters of the Coulomb interaction in the compression process by precise numerical simulations and analytical analyses. We have identified three stages to describe the dynamical evolution of the Coulomb interaction in the compression process, which is beyond the ballistic compression model. In combination with a novel sub-fs jitter correction approach, our work will shed light on improving the temporal resolution to a few fss and even attosecond timescales in probing with electrons with arbitrary kinetic energies.

2. Dynamical suppression of the Coulomb interaction in the compression process

The layout of the RF compression UED is shown in figure 1(a), and more details regarding this system can be found elsewhere [31]. The initial electron pulse contains 10^5–10^6 electrons with a duration of 90 fs

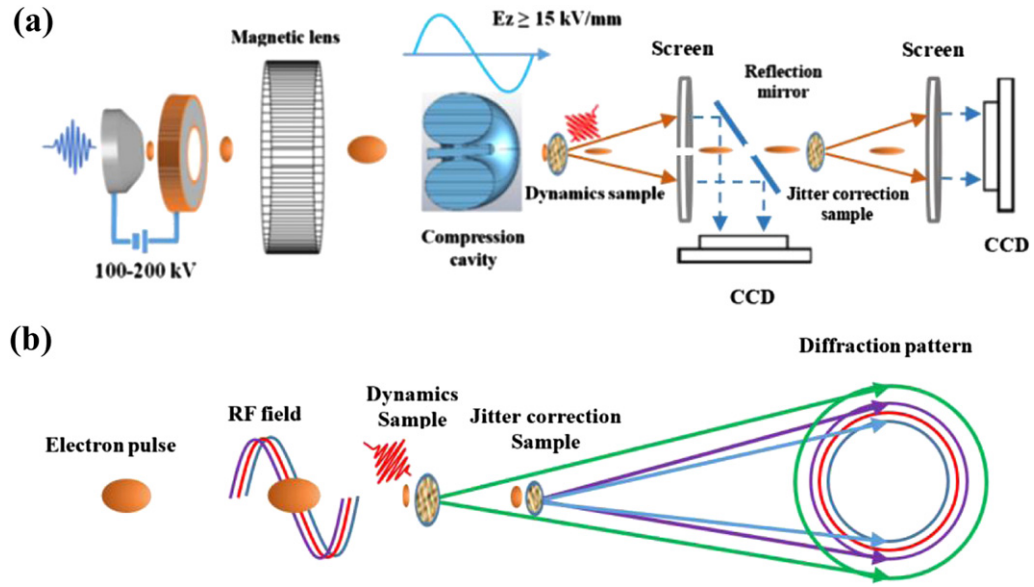

Figure 1. (a) The layout of the RF-compression UED and the jitter correction approach. The photoelectron pulses are accelerated to 100–200 kV and collimated by the magnetic lens, and then compressed by the compression cavity. The dynamics sample is placed at the temporal focus position. At variable time delays, diffraction patterns are recorded by the first CCD camera. The unscattered zero order beam passes through the center holes of the screen and the reflection mirror, is then diffracted by the jitter correction sample. The static diffraction pattern for jitter correction is recorded by the second CCD camera. (b) The schematic of the jitter correction approach. The energy of the compressed electron pulse is sensitive to the phase and amplitude jitters under a strong compression field. The energy shift of the electron pulse can be determined by fitting the change of the diffraction peak position of the jitter correction sample. Then the phase jitter is retrieved from the static diffraction pattern. Here is an alternative layout that one CCD camera records both the diffraction patterns from the jitter correction sample and the dynamics sample.

Table 1. Summary of the parameters and the simulation results in the text.

Parameters	Case 1	Case 2	Case 3
Electrons per pulse	10^5	10^5	0.5×10^6
Electron pulse energy	100 kV	100 kV	200 kV
Duration before compression (RMS)	495 fs	240 fs	360 fs
Distance between photocathode and cavity	12 cm	7 cm	8 cm
RF field strength	5.3 kV mm^{-1}	16.8 kV mm^{-1}	33.6 kV mm^{-1}
Distance from cavity to temporal focus	6.1 cm	1.6 cm	2.6 cm
Electron pulse duration (RMS)	16.3 fs	4.1–6.1 fs	7.6 fs
Transverse spotsize (RMS)	156 μm	115 μm	176 μm
Transverse coherence	1.7 nm	1.0 nm	1.2 nm
Wavelength spread (from RMS energy spread)	0.21%	0.38%	0.40%
Divergence	0.15 mrad	0.41 mrad	0.31 mrad
Jitter amplification factor	1.77	1.32	1.22
Jitter correction precision	2.46 fs	0.78 fs	0.39 fs

(FWHM). The energy spread of the electron pulse is 0.1 eV and the transverse spotsize is 100 μm RMS with a Gaussian distribution. The electron pulse is accelerated to 100–200 keV by a static field strength of 10 kV mm^{-1}, then the magnetic lens focuses and collimates the electron pulse into the RF compression cavity. The RF cavity operates in the TM_{010} mode with the central frequency of 3.2 GHz [31]. The beam dynamics during the propagation is simulated by general particle tracer [43] with a 3D space charge model. The 3D configurations and dimensions of the RF compression cavity and the magnetic lens are from actual elements in our home-made UED system [31], and the electric and magnetic field distributions produced by these elements are calculated by Poisson Superfish [44]. The initial parameters and the simulation results for three selected cases are summarized in table 1. Comparing with case 1, the pulse duration is further compressed to 6.1 fs RMS in case 2 with a shorter distance of 7 cm between the photocathode and the compression cavity. The shorter distance suppresses the degeneration of the compression ability from the nonlinear curvature of the compression field [21, 27]. Figure 2(a) shows the evolution of the electron pulse duration as a function of the propagation distance at different RF field strength under the case 2 condition. With a compression field of 16.8 kV mm^{-1}, the pulse duration is compressed to the minimum rapidly to a shorter duration than that of the initial pulse. The relative energy spread of 0.38% in case 2 is on the same

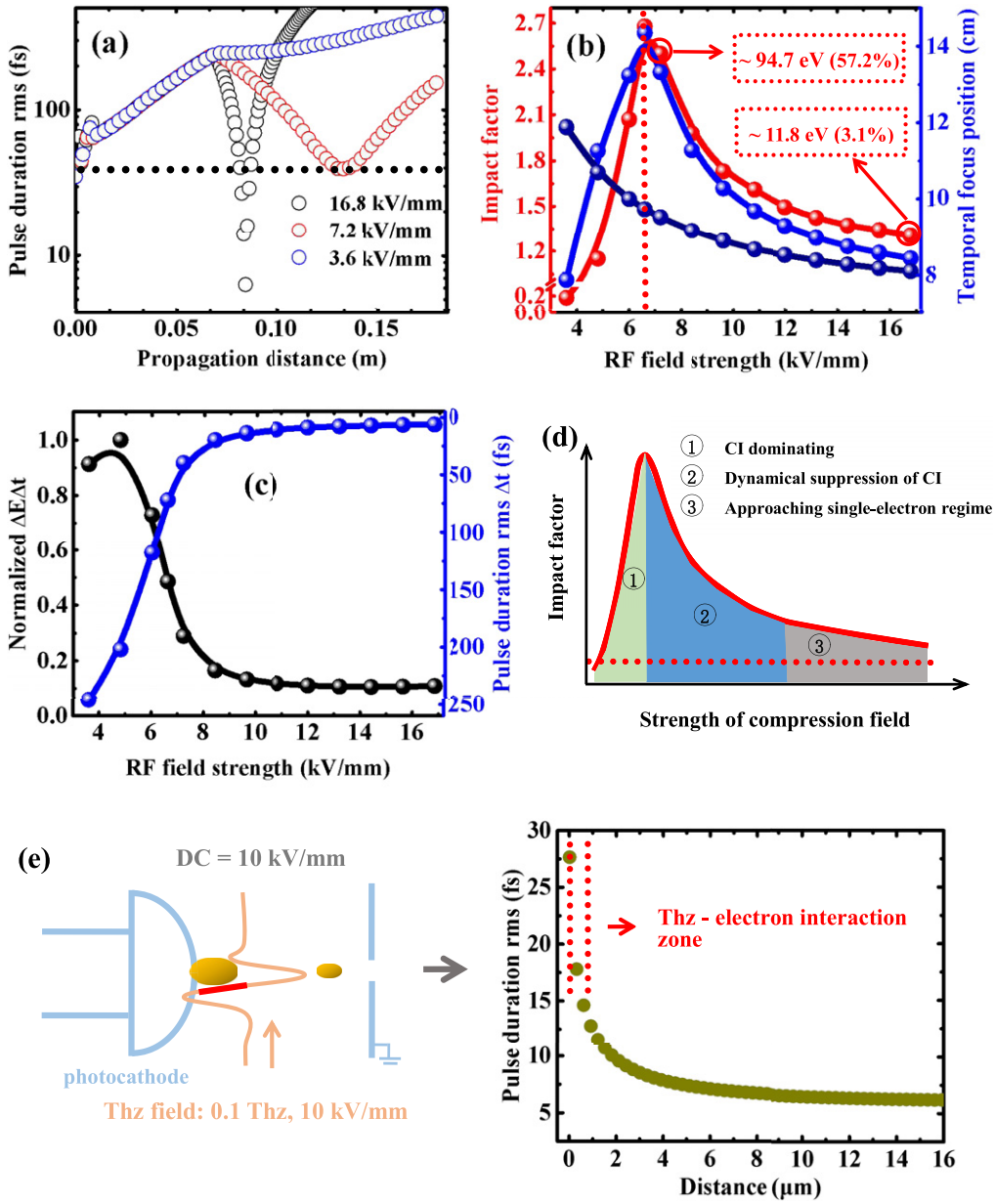

Figure 2. The dynamical suppression and the energy independence of Coulomb interaction in compression. (a) The pulse duration as a function of the propagation distance and the compression field strength in case 2 of table 1. The dotted line represents the initial electron pulse duration around the photocathode. (b) The impact factor (red balls) and the temporal focus position (blue balls) as a function of the compression field strength. The dark blue balls and the light blue balls denote the evolution from the analytical model and the numerical simulation respectively. The dotted vertical line indicates the peak position of the track of the impact factor. (c) The evolution of the pulse duration and the normalized $\Delta E\Delta t$ as field strength increasing. The value $\Delta E\Delta t$ denotes the required energy spread ΔE for compression to a finite pulse duration Δt. (d) The schematic illustration of the three stages in the compression of electron pulse. CI is the abbreviation of the Coulomb interaction. The dotted line indicates the ideal condition that the impact factor is 1. (e) An exemplify of the energy independence of the coulomb interaction in compression. By a THz compression at surface of photocathode, the electron pulse containing 10^5 electrons is compressed to ~6 fs RMS with the kinetic energy of 150 eV and a temporal focus of 15 μm.

level as that in the moderate compression [28, 31, 35]. The transverse spotsize at the temporal focus position is 100–200 μm RMS, meeting the general requirement in UED experiment. In addition, the simulation results indicate that the strong Coulomb force does not give rise to a significant emittance growth in this drastic compression as shown in table 1 and the transverse coherence length of 1–2 nm retains the initial value at the photoemission.

Generally, the Coulomb interaction make the compression deviate from the analytical model [26, 45] where the Coulomb interaction is neglected. A typical problematic-parameter is the temporal focus distance. A recent study [31] shows that the Coulomb interaction extends the temporal focus distances to 2–3 times larger than that calculated by the analytical model. Here we take the ratio between the experimental (or simulated) temporal focus distance and the analytical temporal focus distance as the

impact factor to quantify the impact of Coulomb interaction on the compression process. The temporal focus distances from the simulation (considering the Coulomb interaction) and the analytical model (neglecting the Coulomb interaction) [26] are s_{sim} and s_{anal} respectively. The ratio s_{sim}/s_{anal} is defined as the impact factor. Figure 2(b) summarizes the results. s_{anal} declines monotonically while s_{sim} climbs up firstly then declines. The evolution trace of the impact factor (red balls) goes up firstly then drops as the field strength increases and finally the impact factor approaches to 1. The initial climbing of the impact factor indicates that the Coulomb interaction impedes the compression and more kinetic energy transforms to the potential energy among electrons. The subsequent decline by further increasing the field strength suggests a suppression of the impact of the Coulomb interaction in compression. At a field strength of 16.8 kV mm^{-1}, 3.1% (11.8 eV) of the kinetic energy chirp transforms to the potential energy as shown in figure 2(b), which is significantly smaller than that of 57.2% (94.7 eV) at the field strength of 7.2 kV mm^{-1}. The nearly switching off of the energy transformation suggests a transition from the stage of Coulomb interaction domination to the stage of impressive Coulomb interaction suppression. A recent work on the ultrafast electron microscopy also shows that the energy spread preserves at the temporal focus plane under the strong compression [30]. To avoid the impact of the transverse distribution to the longitudinal compression, the transverse spotsize and the divergence of the electron pulse are kept at the same value in the numerical simulations by tuning the current of the magnetic lens. The conservation of the phase space in single-electron pulse compression indicates $\Delta E\Delta t$ is constant and equal to the initial value at the photoemission. By taking into account the Coulomb interaction, the descending of $\Delta E\Delta t$ by one order of magnitude in figure 2(c) denotes less energy spread ΔE is required for the compression to a smaller pulse duration Δt, which coincides with the suppression of Coulomb interaction by increasing the compression field strength. Note that this suppression effect is pervasive in both the moderate compression [31] and the drastic compression discussed here.

In regard to the mechanism of the suppression of the Coulomb interaction, we discuss in two aspects, namely the Coulomb force and the temporal focus distance. We calculated the longitudinal electric field distributions of the electron pulse before the compression and at the temporal focus by numerical simulations as shown in the appendix A. We find that, in the compression process, the longitudinal distribution of the electric field is nearly unchanged and is independent of the pulse duration. In the analytical model [21, 46], the Coulomb field scales as $Ez \propto \zeta/L$, where ζ is the longitudinal position of the electron inside an electron pulse and L is the pulse length. The static distribution of the Coulomb field Ez is hence constant and independent on the pulse length, which coincides with the simulation results. As the compression field strength increases, the large velocity chirp shortens the temporal focus distance as shown in figures 2(a) and (b). The combination of the constant Coulomb field and the reduced temporal focus distance (shorter travel time) reduces the overall Coulomb interaction and gives rise to the dynamical suppression effect of the Coulomb interaction.

Based on the dynamical suppression of the Coulomb interaction, we identify three stages in the electron pulse compression as shown in figure 2(d). The first stage is a Coulomb interaction dominated compression with a low compression field strength, where a large amount of the energy chirp transforms to the Coulomb potential energy. In the second stage, the Coulomb interaction is dynamically suppressed as the compression field strength increases. The energy transformation nearly switches off in the third stage and the compression of high-charge electron pulse approaches the single-electron pulse compression regime. The widely used moderate compression [31] belongs to the second stage while the drastic compression of the electron pulse duration to far below the duration of the photoemission laser in this work belongs to the third stage.

3. The energy independence of the Coulomb interaction in compression

Both the Coulomb force and the temporal focus distance are related to the kinetic energy of electron pulse, while the dependence of the Coulomb interaction on energy is not clear. If neglecting the Coulomb interaction, the relative position shift Δl of two particles along the longitudinal direction can be given by $\Delta l = \int_0^s \frac{\Delta\beta}{\beta}\,\mathrm{d}z$ integrating from the position of compression field (i.e. $z = 0$) to the temporal focus position (i.e. $z = s$), where β and $\Delta\beta$ represent the average velocity and the velocity difference [21]. The linear term of the Taylor expansion of $\frac{\Delta\beta}{\beta}$ is $\frac{\Delta\gamma}{\beta^2\gamma^3}$, where γ and $\Delta\gamma$ represent the average energy and the energy spread in terms of the relativistic Lorentz factor, then

$$\Delta l \approx \int_0^s \frac{\Delta\gamma}{\beta^2\gamma^3}\,\mathrm{d}z. \tag{1}$$

The average velocity β and the average energy γ will not change in the compression process. So

$$\Delta l \approx \int_0^s \frac{\Delta\gamma}{\beta^2\gamma^3}\,\mathrm{d}z = \int_0^{s\beta^2\gamma^3} \Delta\gamma d\left(\frac{z}{\beta^2\gamma^3}\right) = \int_0^{s\beta^2\gamma^3} \Delta\gamma dz' = \int_0^{s'} \Delta\gamma dz' \tag{2}$$

where $s' = s\beta^2\gamma^3$, involving the contribution from β and γ. In this case, $dz' \propto \beta^2\gamma^3$. As shown in figure 2(b), the Coulomb interaction prolonged temporal focus distance s_{sim} is just larger than the analytically calculated s_{anal} by less than three times. So the proportion $dz' \propto \beta^2\gamma^3$ still holds under the impact of the Coulomb interaction. The relativistic effect diminishes the Coulomb force by $F_c = qE_c/mc^2\beta^2\gamma^3$ (page 296 in reference [47]), where q and m are the electron charge and the mass respectively and E_c is the Coulomb electric field. Then

$$F_c \propto \beta^{-2}\gamma^{-3}. \tag{3}$$

During the compression, the Coulomb interaction does not change β and γ. Under this circumstance, the Coulomb interaction (CI) integrating Coulomb force within temporal focus distance, i.e. CI $= \int_0^{s'} F_c \mathrm{d}z'$, is energy-independent. The physical scenario is that, with a definite compression ratio, the electron pulse with the low kinetic energy and the high static Coulomb force goes to the very close temporal focus position promptly, while the electron pulse with the high kinetic energy and the low static Coulomb force goes a long distance to the temporal focus position. Therefore, both the low and the high energy electron pulses undergo an equivalent Coulomb interaction when propagating to their respective temporal focuses.

To testify this energy independence, we perform a simulation of THz compression of low energy electrons and results are shown in figure 2(g). The single-cycle THz field with the frequency of 0.1 THz is positioned at the photocathode surface to maintain the compression at the low kinetic energy. The electron pulse containing 10^5 electrons is accelerated by both the DC field and the single-cycle THz field. A linear part of the THz field with the field strength of 10 kV mm^{-1} is selected to introduce the energy chirp on the electron pulse. The initial 30 fs RMS pulse duration is compressed to ~6 fs RMS at the 15 μm position after the photocathode. The kinetic energy of the electron pulse is ~150 eV and the energy spread induced by the THz field is ~0.27 eV at the temporal focus. Recently, a simulation on the laser pulse shaping induced electron pulse self-compression shows that a compression finishes within one micrometer [17] (notice that the horizontal axis in figure 3(d) in this paper should be μm as depicted in the text). In this study, the electron pulse containing 2×10^4 electrons is compressed to several fss while the kinetic energy is still below 1 eV. These two examples of compressing ultralow energy electron pulses unambiguously evidence the energy independence of Coulomb interaction in compression. In other words, the eV and MeV electron pulses suffer the same amount of Coulomb interaction in the compression process.

4. The microscale suppression of the Coulomb interaction within an electron pulse

Though the Coulomb interaction is dynamically suppressed, the decline of the pulse duration slows down gradually as shown in figure 2(c). The compressed pulse duration keeps nearly unchanged by further increasing the compression field strength to 16 kV mm^{-1} and above. Figure 3(a) presents the longitudinal phase space (B_z vs T) at the temporal focus position with a radial color coding. From the inner to the outer radius, the corresponding electrons go through the under-compression (blue dots), the compression (green dots) and the over-compression (red dots). The inner radius electrons with a high density suffer larger Coulomb repulsive force, inducing a longer temporal focus distance than that of the outer radius. The inset in figure 3(a) shows the temporal distribution of 8 segments separated along radial direction. Each segment represents 12.5% of total electrons. From the outer to the inner radius, the temporal distribution of each segment changes from 10 fs RMS to 4 fs RMS. However, even for the centermost electrons, the 4 fs RMS distribution is comparable to the 6.1 fs RMS distribution of all electrons. So the transverse distribution influences the compression ability but does not play a decisive role. Electrons on the same radius form an S-shape distribution in the longitudinal direction, such as the blue dots in figure 3(a), where the head and the tail electrons are crossing (i.e. over-compression) while the center electrons are still under-compression. The S-shape distribution exists pervasively in compressed MeV electron pulses [9, 21, 27, 48, 49]. We have clearly shown in figure 2(b) that the overall Coulomb interaction that an electron pulse suffers in compression is dynamically suppressed by increasing the compression field strength. As an analogy, within the electron pulse, the head (tail) electrons with higher energy spread may suffer less Coulomb interaction than that of the center electrons in the compression process. Based on this concept, we propose a microscale suppression of the Coulomb interaction within a single pulse to explain the S-shape distribution and the degeneration of the compression ability. The schematic is shown in

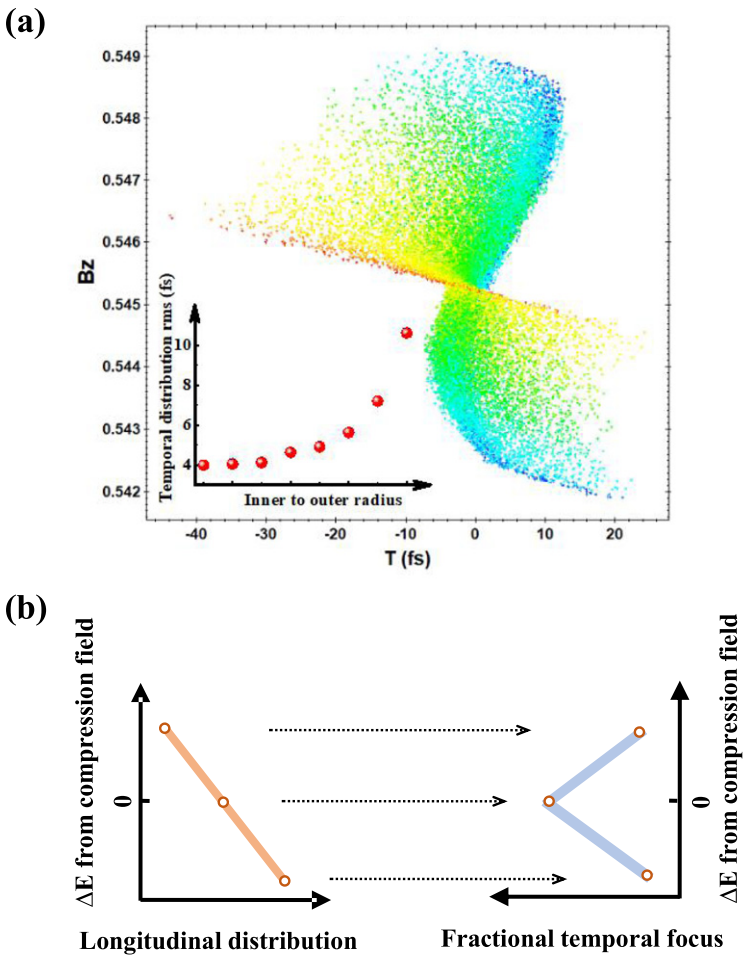

Figure 3. The limitation of the compression ability by the dynamical suppression of Coulomb interaction in single pulse. (a) At the temporal focus position of case 2, the distribution of the normalized longitudinal velocity B_z (i.e. v_z/c) with the arrival time T. The electrons are color-coded from the inner (the blue) to the outer radius (the red). The inset is the temporal distribution of the electrons from inner to outer radius, which is separated into 8 segments equally. (b) The schematic of the degeneration of the compression ability by the dynamical suppression of Coulomb interaction in single pulse. The front (tail) electrons loss (gain) more energy from compression field than that of the center electrons (in the left figure), then the front (tail) electrons suffer less Coulomb interaction in the compression. A fractional temporal focus is formed in single pulse (in the right figure) where the temporal focus of the front and tail electrons is shorter than that of the center electrons.

figure 3(b). The front (tail) electrons loss (gain) more kinetic energy from the compression field than that of the center electrons, therefore these electrons suffer less Coulomb interaction than that of the center electrons in the compression process. As a consequence, a fractional temporal focus is formed in single pulse where the temporal focus distance of the front and tail electrons is shorter than that of the center electrons, giving rise to the S shape distribution and a significant degeneration of the compression ability.

Note that the previous studies [21, 28, 48] seek for a linear Coulomb field distribution in three dimensions and attribute the degeneration of the compression ability to the nonlinear Coulomb force and the nonlinear energy chirp. The dynamical suppression of the Coulomb interaction in microscale in single pulse deviates the compression from the ideal linear concept and provides a new perspective to view the compression ability. The microscale suppression effect may associate with the mechanism of the nonlinear time-energy compression in single-spike x-ray pulses [9]. Besides the microscale suppression effect, a high order nonlinear term of the compression field [21] may play a minor role in contributing to the S-shape phase space. Tuning the electron density and phase space can compensate the microscale suppression effect and enable a further compression to attosecond, which will be explored in future work.

5. Stamping the timing jitter by recording statistic diffraction patterns

The phase jitter and the amplitude jitter of the compression field accelerate or decelerate electron pulses. The corresponding energy change can be accurately determined by fitting the Bragg peak position in a diffraction pattern. We present a jitter correction approach by taking statistic diffraction patterns and the

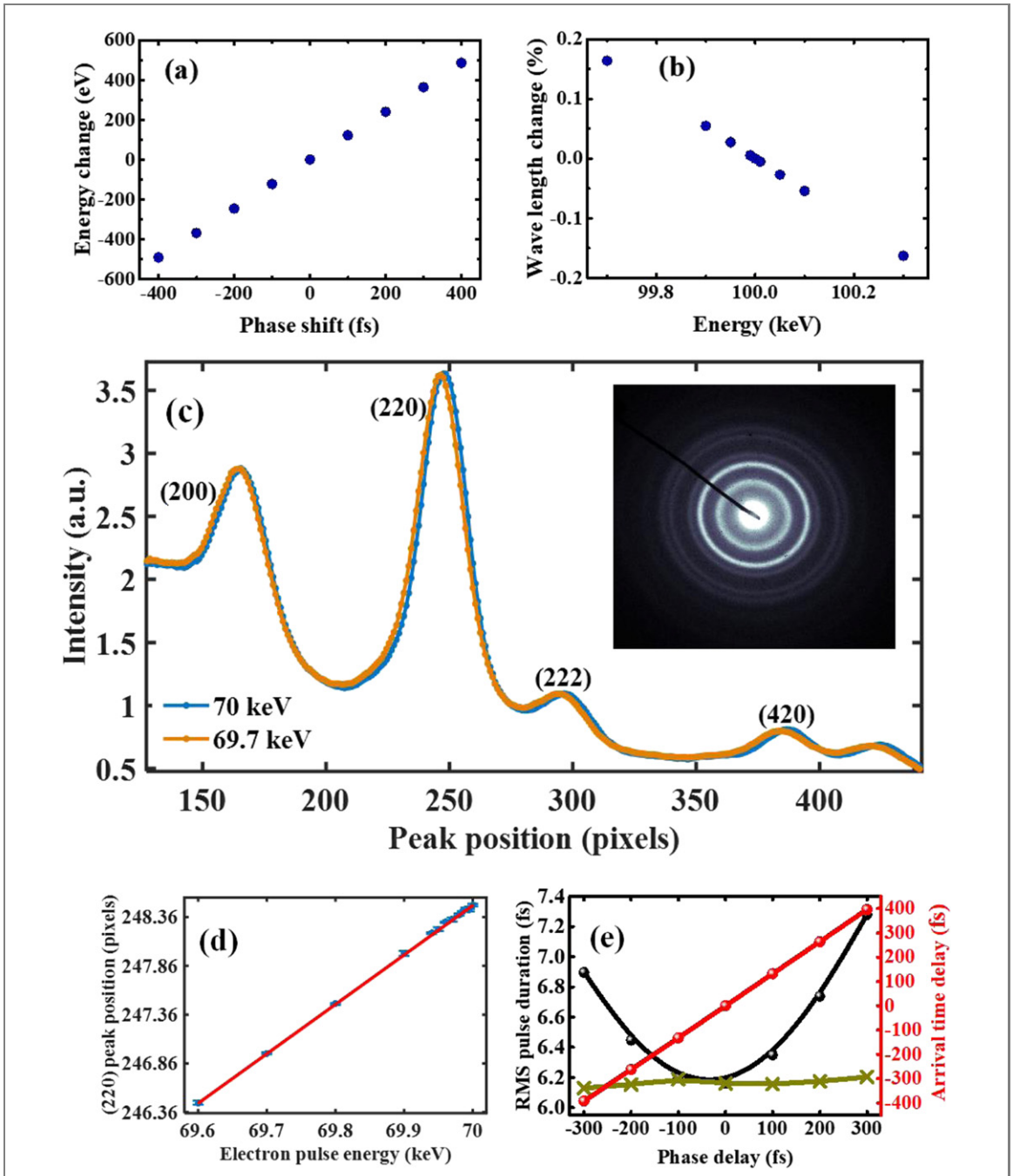

Figure 4. For the compression condition in case 1, (a) the kinetic energy of the electron pulse varies linearly with the shift of the RF phase by a ratio of 1.22 eV fs^{-1}. (b) The linear relationship between the electron pulse energy and the corresponding change of the electron wavelength ($\Delta\lambda/\lambda$) in percentage. (c) The diffraction pattern of $Ge_2Sb_2Te_5$ (inset) and the radial average. The diffraction peak position shifts by changing the DC voltage. (d) The measured linear ratio between the electron pulse energy and the corresponding peak position shift is 0.005 pixel/eV. The standard deviation of the fitted peak position at fixed energy is below 0.015 pixel. (e) The black balls and the brown crosses represent the evolutions of the pulse duration as a function of RF phase shift at the fixed temporal focus position (i.e. 1.6 cm away from the cavity) and varied temporal focus positions in the compression condition of case 2. The red spots show the linear relationship between the RF phase shift and the arrival timing jitter at the sample position. The linear ratio, i.e. the jitter amplification factor, is 1.32.

two schemes are shown in figures 1(a) and (b) respectively. In figure 1(a), the first CCD camera records the time-resolved diffraction information of the dynamical sample. The zero order (or unscattered) electrons, passing through the center holes on the screen and the reflection mirror, are diffracted by the jitter correction sample. The static diffraction pattern from the jitter correction sample is recorded by the second CCD camera for stamping the jitter of each shot. This jitter correction approach is non-invasive by recording the jitter and the dynamical structure information at the same time but on different CCD cameras. In figure 1(b), one CCD camera records both the diffraction patterns from the dynamical sample and the jitter correction sample on the same image. We test the jitter correction approach by the following simulation and experiment. The compression condition of case 1 in table 1 is taken as an example. The

phase jitter of the compression field will transfer linearly to the kinetic energy change of the electron pulse by a ratio of 1.22 eV fs^{-1} as shown in figure 4(a). For conditions of case 2 and case 3, the linear ratios are 3.87 eV fs^{-1} and 7.73 eV fs^{-1} respectively. Figure 4(b) depicts the linearly dependence of the electron wave length ($\Delta\lambda/\lambda$) on the kinetic energy of electron pulse. As a consequence, the phase jitter changes the wavelength of the electron pulse linearly. For a static electron diffraction pattern, the Bragg peak position R on the screen is proportional to the electron de Broglie wavelength λ as:

$$R = L\lambda/d \tag{4}$$

where R is the distance from the unscattered center spot to the diffraction spot or ring on the camera, d is the interplanar spacing, L is the distance between the sample and the camera. Therefore, the Bragg peak position shifts linearly with the electron wavelength in the formula. Combining with the linear relationship between phase jitter and wavelength, we illustrate the linear dependence of Bragg peak position on the phase jitter of compression field. A proof-of-principle experiment was carried out on our compact UED system [12]. The sample is a thin film poly-crystalline phase change material $Ge_2Sb_2Te_5$ in the rock-salt phase with a thickness of 15 nm. The typical diffraction pattern and the radially averaged 1D intensity curves at the DC voltage of 69.7 kV and 70 kV are shown in figure 4(c). As tuning the DC voltage linearly, the peak position of (220) presents a linear shift as shown in figure 4(d). The ratio between the electron pulse energy change and the peak position shift is 0.005 pixel/eV and the standard deviation (std) of the fitted peak position is $\leqslant$0.015 pixel. So the energy resolution in this case is better than 3 eV (std). In accordance with the linear ratio of 1.22 eV fs^{-1} in case 1, 3.87 eV fs^{-1} in case 2, and 7.73 eV fs^{-1} in case 3, the jitter correction precision (std) is better than 2.46 fs, 0.78 fs and 0.39 fs respectively. Notice that the impact of the $\leqslant$1 eV voltage ripple from the DC voltage source (Heinzinger PNChp series) can be excluded in this measurement.

In the above measurement, about 10^8 electrons were accumulated for each image to obtain a high signal-to-noise ratio. In contrast, the compressed pulse of 10^5 electrons in case 2 will not provide sufficient number of electrons per pulse to retain both the few-fs pulse duration and the sub-fs jitter stamping. To maintain the precision of the time stamping, besides further increasing the electron number, an alternative way is to scatter more electrons by increasing the thickness of the jitter correction sample. In addition, single crystalline film will benefit the signal-to-noise ratio of which a diffraction pattern is composed of isolated bright spots rather than Debye–Scherrer rings in poly-crystal. A proper choose of the type of the material for jitter correction which can scatter more electrons and a direct electron detection camera with higher detective efficiency [50] are also helpful. Besides stamping the jitter shot by shot, the long-term drift can also be stamped in the accumulation mode, in particular for the electron pulse compression by the THz [23, 51] and the laser field [52] where the synchronization is intrinsic but perturbed by the environment in a short timescale.

We also simulated the impact of the phase (and the amplitude) jitter to the compression ability and the results are presented as follow. In the compression condition of case 2, a 300 fs phase shift yields a negligible variation of the compressed pulse duration from ~6 fs RMS to ~7 fs RMS at the fixed temporal focus position, as shown in figure 4(e) (the black balls). A 200 fs phase shift of the compression field will introduce a ~0.3% change of the diffraction peak position in case 2, which needs to be noticed in a precise measurement such as the transient peak position change by laser excitation. Nevertheless, this jitter induced peak position fluctuation can be readily corrected by the abovementioned jitter correction approach. The stamped jitter derives from the energy fluctuation of the electron pulse so it represents the phase and the amplitude jitter of the compression field. The arrival timing jitter of the electron pulse at the sample position is always larger than the phase jitter due to the Coulomb interaction during the compression, dubbed as the jitter amplification effect [31]. As shown in figure 4(e), the jitter amplification factor, i.e. the slope of the red spots, is 1.32, which suggests that the arrival timing jitter at the sample position is 1.32 times larger than the RF phase jitter. Overall, the drastic compression is robust and not sensitive to the phase and amplitude jitters of the compression field.

6. Discussion and conclusions

By taking into account the dynamical suppression of the Coulomb interaction, we identify three stages for describing the compression process. Several points are worth mentioning based on the three stages in electron pulse compression. Firstly, the Coulomb interaction virtually produce no deterioration on the compression till to the drastic compression regime. The misleading 'adverse effect' of Coulomb interaction on compression ability [19, 24] is derived from inappropriate experimental operations. Measuring the compressed pulse duration at fixed field strength [19] or fixed temporal focus position [24] is improper on

characterizing the compression ability, because the Coulomb interaction introduces an energy chirp before the compression which alters the requiring field strength and the temporal focus position significantly in the subsequent compression. Secondly, the puzzling transformation of the phase space in energy and time in reference [30] can be well described by the dynamical suppression effect of the Coulomb interaction and the identified three stages in electron pulse compression. Thirdly, the dynamical suppression of Coulomb interaction in the compression process potentially lowers the increase of the transverse emittance and may inspire the exploration on the compression of ultracold electron pulses [53]. The identified three stages for describing the electron pulse compression is beyond the ballistic compression model and the energy transformation model in three aspects: the first is that the Coulomb interaction and the dynamical evolution of the Coulomb interaction are involved; the second is that it can be used to describe the drastic compression; the third is that it well depicts the switching off of the energy transformation [30] and the jitter amplification effect [31].

We discuss two potential applications and advancements based on the revealed three characters of the Coulomb interaction in compression. One is the drastic compression of the low energy electron pulse. As the Coulomb interaction is energy independent, i.e. the eV and MeV electron pulse suffer the same amount of the Coulomb interaction for a defined compression ratio, eV electron pulse holds the same compression ability as that of the conventional keV and MeV electron pulses. The compressed low energy electron pulse can be used to probe surface chemistry [54] and two-dimensional material system [55] in the back scattering and the transmission mode. The other one is the drastic compression to the Fourier limit. The dynamical suppression of the Coulomb interaction indicates that with the drastic compression, the Coulomb interaction introduces a negligible impact to the energy chirp gained from the compression field, i.e. the compression approaches the single-electron compression regime as depicted in the three stages of electron pulse compression. Moreover, in figure 2(e), the energy spread of 0.27 eV and the pulse duration of 6 fs at the temporal focus position enable a Fourier-limited electron pulse, i.e. $\Delta E\Delta t \sim \hbar/2$, a time bandwidth product near the Fourier transform limit. The Fourier-limited electron pulse will benefit the electron energy loss spectroscopy with meV–fs resolution in study of the bonding dynamics [56]. Finally, we discuss the impact of our work on the Coulomb interaction to the field of electron pulse compression. The recent advancement shows that attosecond pulse trains have been achieved by the optical field compression [57–60], however, most studies focus on the compression of single-electron pulse, avoiding the Coulomb interaction. Our work on quantifying the impact of Coulomb interaction in electron pulse compression provides a general physical scenario in extending the microbunched pulse trains to the multi-electron microbunching regime.

In this work, a deep insight into the Coulomb interaction and three characters in the compression of electron pulse are presented. The dynamical suppression and the energy independence of the Coulomb interaction indicate a real manipulation of the Coulomb interaction by compression. Three stages are identified for describing the compression process, which is beyond the ballistic compression model. The reveal of the microscale suppression of the Coulomb interaction and the noninvasive jitter correction approach shed light on improving the temporal resolution to a few fss and attosecond in probing with electrons with arbitrary kinetic energy.

Acknowledgments

This work has been partially supported by National Natural Science Foundation of China (Nos. 11727810 and 61720106009), the Science and Technology Commission of Shanghai Municipality (No. 19JC1412200) and the Program of Introducing Talents of Discipline to Universities 111 project (B12024), and National Natural Science Foundation of China (No. 11974241). Yingpeng Qi acknowledges the support by the Sino-German (CSC-DAAD) Postdoc Scholarship Program (Grant No. 201709920054 and No. 57343410) and the funding from Max Plank Society.

Appendix A. The Coulomb field distribution in single pulse before and after compression

We discuss the electric field distribution before and after the compression. Fig. A1(a) shows the linear distribution of the electric field *fEz* along the longitudinal direction before compression in single electron pulse in case 2. At the temporal focus position, the std (*fEz*) and the sum (*fEz*) of the electron pulse compressed to 6.1 fs RMS by field strength of 16.8 kV mm^{-1} in figure A1(c) are comparable to that of the compression to ∼40 fs RMS by the field strength of 7.2 kV mm^{-1} in figure A1(b). More

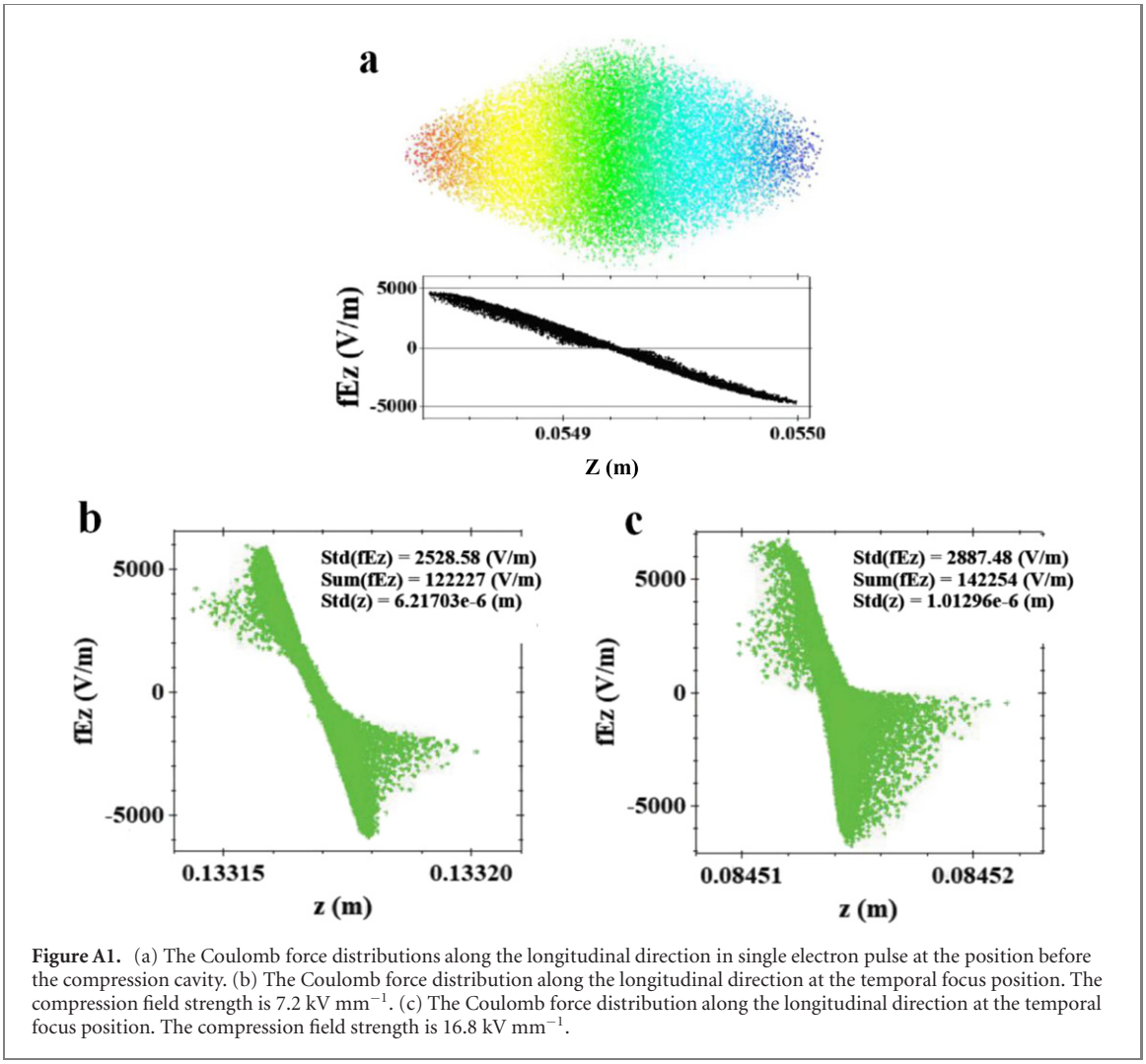

Figure A1. (a) The Coulomb force distributions along the longitudinal direction in single electron pulse at the position before the compression cavity. (b) The Coulomb force distribution along the longitudinal direction at the temporal focus position. The compression field strength is 7.2 kV mm^{-1}. (c) The Coulomb force distribution along the longitudinal direction at the temporal focus position. The compression field strength is 16.8 kV mm^{-1}.

generally, the longitudinal distribution of the electric field is nearly constant and independent on the pulse duration.

ORCID iDs

Yingpeng Qi https://orcid.org/0000-0001-5950-8157
Yan Yang https://orcid.org/0000-0003-3769-693X
Haitao Sun https://orcid.org/0000-0003-1471-8876

References

[1] Miller R J D 2014 Femtosecond crystallography with ultrabright electrons and x-rays: capturing chemistry in action *Science* **343** 1108
[2] Elsaesser T and Woerner M 2014 Perspective: structural dynamics in condensed matter mapped by femtosecond x-ray diffraction *J. Chem. Phys.* **140** 020901
[3] Park H, Wang X, Nie S, Clinite R and Cao J 2005 Mechanism of coherent acoustic phonon generation under non-equilibrium conditions *Phys. Rev.* B **72** 100301(R)
[4] Schäfer S, Liang W and Zewail A H 2011 Structural dynamics of nanoscale gold by ultrafast electron crystallography *Chem. Phys. Lett.* **515** 278
[5] Liang W X, Vanacore G M and Zewail A H 2014 Observing (non) linear lattice dynamics in graphite by ultrafast kikuchi diffraction *Proc. Natl Acad. Sci.* **111** 5491
[6] Nie S, Wang X, Park H, Clinite R and Cao J 2006 Measurement of the electronic Gruneisen constant using femtosecond electron diffraction *Phys. Rev. Lett.* **96** 025901
[7] Sciaini G *et al* 2009 Electronic acceleration of atomic motions and disordering in bismuth *Nature* **458** 7234
[8] Rajeswari J *et al* 2015 Filming the formation and fluctuation of skyrmion domains by cryo-Lorentz transmission electron microscopy *Proc. Natl Acad. Sci.* **112** 14212
[9] Huang S *et al* 2017 Generating single-spike hard x-ray pulses with nonlinear bunch compression in free-electron lasers *Phys. Rev. Lett.* **119** 154801

[10] Sciaini G and Miller R J D 2011 Femtosecond electron diffraction: heralding the era of atomically resolved dynamics *Rep. Prog. Phys.* **74** 096101
[11] Siwick B J, Dwyer J R, Jordan R E and Miller R J D 2004 Femtosecond electron diffraction studies of strongly driven structural phase transitions *Chem. Phys.* **299** 285
[12] Waldecker L, Bertoni R and Ernstorfer R 2015 Compact femtosecond electron diffractometer with 100 keV electron bunches approaching the single-electron pulse duration limit *J. Appl. Phys.* **117** 044903
[13] Petruk A A, Pichugin K and Sciaini G 2017 Shaped cathodes for the production of ultra-short multi-electron pulses *Struct. Dyn.* **4** 044005
[14] Aidelsburger M, Kirchner F O, Krausz F and Baum P 2010 Single-electron pulses for ultrafast diffraction *Proc. Natl Acad. Sci.* **107** 19714
[15] Zhu P F *et al* 2015 Femtosecond time-resolved MeV electron diffraction *New J. Phys.* **17** 063004
[16] Wang X J, Qiu X and Zvi I B 1996 Experimental observation of high-brightness microbunching in a photocathode rf electron gun *Phys. Rev.* E **54** R3121(R)
[17] Qi Y P *et al* 2015 Realizing ultrafast electron pulse self-compression by femtosecond pulse shaping technique *J. Phys. Chem. Lett.* **6** 3867
[18] Baum P and Zewail A H 2007 Attosecond electron pulses for 4D diffraction and microscopy *Proc. Natl Acad. Sci.* **104** 18409
[19] Fill E, Veisz L, Apolonski A and Krausz F 2006 Sub-fs electron pulses for ultrafast electron diffraction *New J. Phys.* **8** 272
[20] Gliserin A, Apolonski A, Krausz F and Baum P 2012 Compression of single-electron pulses with a microwave cavity *New J. Phys.* **14** 073055
[21] Floettmann K 2014 Generation of sub-fs electron beams at few-MeV energies *Nucl. Instrum. Methods Phys. Res.* A **740** 34
[22] Wong L *et al* 2015 All-optical three-dimensional electron pulse compression *New J. Phys.* **17** 013051
[23] Kealhofer C, Schneider W, Ehberger D, Ryabov A, Krausz F and Baum P 2016 All-optical control and metrology of electron pulses *Science* **352** 429
[24] Gliserin A, Walbran M, Krausz F and Baum P 2015 Sub-phonon-period compression of electron pulses for atomic diffraction *Nat. Commun.* **6** 8723
[25] Siwick B J, Dwyer J R, Jordan R E and Miller R J D 2002 Ultrafast electron optics: propagation dynamics of femtosecond electron packets *J. Appl. Phys.* **92** 1643
[26] Pasmans P L E M, van den Ham G B, Dal Conte S F P, van der Geer S B and Luiten O J 2013 Microwave TM_{010} cavities as versatile 4D electron optical elements *Ultramicroscopy* **127** 19
[27] Maxson J *et al* 2017 Direct measurement of sub-10 fs relativistic electron beams with ultralow emittance *Phys. Rev. Lett.* **118** 154802
[28] Van Oudheusden T *et al* 2007 Electron source concept for single-shot sub-100 fs electron diffraction in the 100 keV range *J. Appl. Phys.* **102** 093501
[29] Van Oudheusden T *et al* 2010 Compression of sub-relativistic space-charge-dominated electron bunches for singleshot femtosecond electron diffraction *Phys. Rev. Lett.* **105** 264801
[30] Williams J *et al* 2017 Active control of bright electron beams with RF optics for femtosecond microscopy *Struct. Dyn.* **4** 044035
[31] Qi Y P *et al* 2017 Coulomb interaction-induced jitter amplification in RF-compressed high-brightness electron source ultrafast electron diffraction *New J. Phys.* **19** 023015
[32] Walbran M, Gliserin A, Jung K, Kim J and Baum P 2015 5-fs laser-electron synchronization for pump–probe crystallography and diffraction *Phys. Rev. Appl.* **4** 044013
[33] Yang H *et al* 2017 10-fs-level synchronization of photocathode laser with RF-oscillator for ultrafast electron and x-ray sources *Sci. Rep.* **7** 39966
[34] Casanova A *et al* 2016 Ultrafast amplifier additive timing jitter characterization and control *Opt. Lett.* **41** 898
[35] Chatelain R P, Morrison V R, Godbout C and Siwick B J 2012 Ultrafast electron diffraction with radio-frequency compressed electron pulses *Appl. Phys. Lett.* **101** 081901
[36] Brussaard G J H, Lassise A, Pasmans P L E M, Mutsaers P H A, van der Wiel M J and Luiten O J 2013 Direct measurement of synchronization between femtosecond laser pulses and a 3 GHz radio frequency electric field inside a resonant cavity *Appl. Phys. Lett.* **103** 141105
[37] Kiewiet F B, Kemper A H, Luiten O J, Brussaard G J H and van der Wiel M J 2002 Femtosecond synchronization of a 3 GHz RF oscillator to a mode-locked Ti:sapphire laser *Nucl. Instrum. Methods Phys. Res.* A **484** 619
[38] Otto M R, René de Cotret L P, Stern M J and Siwick B J 2017 Solving the jitter problem in microwave compressed ultrafast electron diffraction instruments: robust sub-50 fs cavity-laser phase stabilization *Struct. Dyn.* **4** 051101
[39] Harmand M *et al* 2013 Achieving few-femtosecond time-sorting at hard x-ray free-electron lasers *Nat. Photon.* **7** 215
[40] Hartmann N *et al* 2014 Sub-femtosecond precision measurement of relative x-ray arrival time for free-electron lasers *Nat. Photon.* **8** 706
[41] Gao M, Jiang Y, Kassier G H and Miller R J D 2013 Single shot time stamping of ultrabright radio frequency compressed electron pulses *Appl Phys. Lett.* **103** 033503
[42] Ruan C Y 2016 Molecular imaging at 1-femtosecond resolution *Science* **354** 283
[43] van der Geer S B and de Loos M J 2016 The general particle tracer code http://pulsar.nl/gpt
[44] Billen J H and Young L M 1996 *Los Alamos National Laboratory Report No. LA-UR-96–1834 (Poisson Superfish)*
[45] van Oudheusden T 2010 Electron source for sub-relativistic single-shot femtosecond diffraction *PhD Thesis* Technische Universiteit Eindhoven
[46] Floettmann K 2017 Emittance compensation in split photoinjectors *Phys. Rev. Accel. Beams* **20** 013401
[47] Wangler T P R F 2008 *Linear Accelerators* 2nd edn (New York: Wiley)
[48] Li R K, Musumeci P, Bender H A, Wilcox N S and Wu M 2011 Imaging single electrons to enable the generation of ultrashort beams for single-shot femtosecond relativistic electron diffraction *J. Appl. Phys.* **110** 074512
[49] Tibai Z, Tóth G, Mechler M I, Fülöp J A, Almási G and Hebling J 2014 Proposal for carrier-envelope-phase stable single-cycle attosecond pulse generation in the extreme-ultraviolet range *Phys. Rev. Lett.* **113** 104801
[50] Lee Y M, Kim Y J, Kim Y J and Kwon O H 2017 Ultrafast electron microscopy integrated with a direct electron detection camera *Struct. Dyn.* **4** 044023
[51] Zhang D *et al* 2018 Segmented terahertz electron accelerator and manipulator (STEAM) *Nat. Photon.* **12** 336
[52] Morimoto Y and Baum P 2018 Diffraction and microscopy with attosecond electron pulse trains *Nat. Phys.* **14** 252

[53] Van Mourik M W, Engelen W J, Vredenbregt E J D and Luiten O J 2014 Ultrafast electron diffraction using an ultracold source *Struct. Dyn.* **1** 034302
[54] Öström H *et al* 2015 Probing the transition state region in catalytic CO oxidation on Ru *Science* **347** 978
[55] Gulde M *et al* 2014 Ultrafast low-energy electron diffraction in transmission resolves polymer/graphene superstructure dynamics *Science* **345** 200
[56] Fabrizio C, Kwon O H and Zewail A H 2010 Dynamics of chemical bonding mapped by energy-resolved 4D electron microscopy *Science* **325** 181
[57] Priebe K E *et al* 2017 Attosecond electron pulse trains and quantum state reconstruction in ultrafast transmission electron microscopy *Nat. Photon.* **11** 793
[58] Kozák M *et al* 2018 Ponderomotive generation and detection of attosecond free-electron pulse trains *Phys. Rev. Lett.* **120** 103203
[59] Black D S *et al* 2019 Net acceleration and direct measurement of attosecond electron pulses in a silicon dielectric laser accelerator *Phys. Rev. Lett.* **123** 264802
[60] Schönenberger N *et al* 2019 Generation and characterization of attosecond microbunched electron pulse trains via dielectric laser acceleration *Phys. Rev. Lett.* **123** 264803